Rhythmic surf zone bars and morphodynamic self organization

Albert Falqués, Nicholas Dodd, Roland Garnier, Francesca Ribas, Laura C. Machardy, Philippe Larroudé, Daniel Calvete, Francisco Sancho

Rhythmic surf zone bars and morphodynamic self-organization

A. Falqués [a,*], N. Dodd [b], R. Garnier [a], F. Ribas [a,1], L.C. MacHardy [b], P. Larroudé [c], D. Calvete [a], F. Sancho [d]

[a] *Applied Physics Department, Technical University of Catalonia, Barcelona, Spain*
[b] *School of Civil Engineering, University of Nottingham, Nottingham, UK*
[c] *LEGI, Université Joseph Fourier, Grenoble, France*
[d] *LNEC, Portugal*

Work undertaken in the EU HUMOR project on morphodynamical modelling, particularly with regard to simulating and understanding rhythmic surf zone bars and related morphodynamic self-organization, is presented. These features are reviewed and their engineering context stated. Hydrodynamical and morphodynamical models developed and/or applied within the HUMOR project in order to address these issues are briefly presented. The linear stability modelling concept and stability studies using fully nonlinear models are contrasted. The stability of a shore-parallel bar under normal or oblique wave incidence is chosen as a test case for the different models. The results are compared and discussed. Lastly, modelling efforts and main results from the project are summarized. Recommendations for further work are made.

Keywords: Surf zone; Morphodynamics; Self-organization; Sand bars; Numerical models; Rhythmic topography; Rip-currents

1. Introduction

The nearshore region frequently exhibits highly complicated motions, and this complexity is perhaps particularly prominent in the intriguing and sometimes confusing changes that can take place in the morphology of many beaches. Descriptions of these complex behaviours abound in the literature, dating back many decades (Evans, 1938; Guilcher et al., 1952; Homma and Sonu, 1962; Sonu, 1972, 1973; Niederoda and Tanner, 1970). An understanding of the physics of such motions has been harder to come by. This is not surprising because the sea bed is constantly being rearranged by water motions that themselves are not fully understood, and the influence of the water motion on the beach (sediment transport) is only partially understood and usually only very crudely describable even now.

One aspect of nearshore morphodynamics that is very intriguing is the observed rhythmicity that seems to occur very frequently, particularly on relatively uninterrupted stretches of sandy coast. In these circumstances so-called transverse/oblique and crescentic bars are frequently observed. The first of these features extend from the shoreline into deeper water, sometimes perpendicular to it, but more commonly at an oblique angle, until they finally blend into the surrounding bathymetry by the middle of the surf zone (see Figs. 1 and 2). Crescentic bars, as their name suggests, are quarter-moon type patterns with the horns of the moon facing shorewards (see Fig. 3). They usually exist fully submerged but can also be observed at low tide.

These patterns, or bed-forms are remarkable in how generic they are, and although the patterns outlined above are idealizations, they can indeed be observed in nature around the world (see, for instance, Wright and Short (1984); Konicki and Holman (2000); Lafon et al. (2002); van Enckevort et al. (2004); Ribas and Kroon (submitted for publication) and references in next section). Both these rhythmic features are therefore natural beach states, at least under certain wave

* Corresponding author.
E-mail address: falques@fa.upc.edu (A. Falqués).
[1] Currently at the Institut de Ciéncies del Mar, CSIC, Barcelona, Spain.

Fig. 1. Rhythmic system of oblique bars in the surf zone of an energetic coast. TrucVert beach, French Atlantic coast.

conditions (see Wright and Short, 1984), and both are also indicative of particular circulation regimes at the shore: crescentic bars are particularly associated with the occurrence of rip channels, which act to transport offshore water that has been deposited at the shore as set-up, and the rips are part of the formation and maintenance of these bed-forms.

Understanding these features is therefore crucial to our knowledge of beach dynamics. In recent years much progress has been made in understanding nearshore morphological changes to the extent that nearshore morphodynamics can be said to have arrived as a discipline in itself. Recent studies (e.g. Blondeaux, 2001) have described some of the basic dynamics that pertain to morphodynamics, and, e.g. Dodd et al. (2003) have described some of the methods used to describe and understand these motions.

Present understanding of rhythmicity in nearshore morphology now tends toward self-organization as most probably describing their occurrence. That is to say that the sea bed and water motion tend to give rise to these states without any imposed pattern (from, perhaps, edge waves (see Holman and Bowen, 1982)). Understanding them is a first step in being able to predict their occurrence. This is important from a very practical point of view, because beaches are a natural sea defence. If we are, for instance, to nourish them, then we must have reasonable confidence that our shoreface nourishment will be redistributed onto the beach face or at least maintained within the surf zone (see Hamm et al., 2002; Spanhoff et al., 2003). If our intention is to maintain tourist beaches then we must be sure that deposited sand is not redistributed in rhythmic beach features. Another important aspect is that rhythmic topography is typically linked to (possibly strong) horizontal circulation with rip-currents which are an important concern for beach safety (Short, 1999). Thus, knowing the morpho- and hydrodynamics in case of rhythmic features is also important for recreational use of beaches.

In this paper we take a look at these issues. We first go into some detail regarding the occurrence of these features worldwide, detailing the many circumstances in which they may be found and their general characteristics. Then we take a look at the present state-of-the-art in modelling them. In particular we focus on so-called self-organizational models of differing type. Such models are in use today to predict beach change, but a review of their use and in particular their success (or otherwise) in reproducing these complicated nearshore features, is lacking. The aim is to give an overview of the models of this type developed (or partially developed) within the EU HUMOR project indicating how they have been applied and illustrating how they can be applied in general. Detailed studies of particular morphologies by using some of these models have already been published elsewhere and the reader is provided here with a brief overview and with the pertinent references. However, a unified description of such models along with a comparison was lacking. For such a comparison the morphodynamic evolution of an initially straight shore-parallel bar is selected as test case. All the models are run over this bathymetry for the same conditions. Results are then compared and discussed, indicating success and failure. Conclusions and a final overall discussion are presented indicating areas of uncertainty and possible ways forward.

2. Rhythmic bars: observations

The nearshore zone exhibits a high diversity of complex but 'regular' topographic patterns and the old attempts of classification become somewhat obsolete as nowadays intensive observations (especially through new techniques like the Argus video cameras system) progress. We will here focus on patterns with the length scale of one to a few times the surf zone width (O(50–1000 m)) and we will discuss two basic types of pattern: transverse/oblique bars and crescentic bars.

2.1. Shore-transverse and oblique bars

These are bars that trend perpendicularly or obliquely to the coast. However, the various descriptions of them in the literature seem to deal with rather different types and it is difficult to state common characteristics apart from their orientation (Komar, 1998; Carter, 1988). They can occur both in sheltered environments (for instance lakes and bays, see Fig. 2) and in open coasts (see Fig. 1). Thus, transverse/oblique bars have been reported from low energy environments

Fig. 2. Rhythmic system of transverse/oblique bars in a low energy beach. Alfacs bay, Ebro delta, Spain.

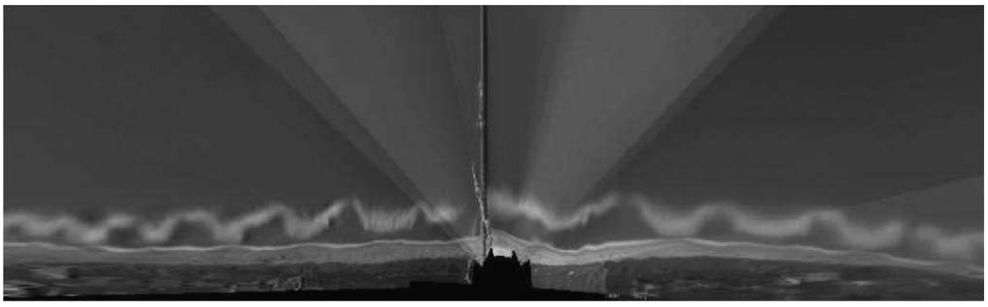

Fig. 3. Crescentic bar, Duck, NC, USA Atlantic coast. Courtesy of Dr. N. Plant and Coastal Imaging Lab, OSU.

(Niederoda and Tanner, 1970; Falqués, 1989) but also from moderate energy coasts like the Lake Michigan (Evans, 1938, 1939), the east US coast (Konicki and Holman, 2000) and the Dutch coast (Ribas and Kroon, submitted for publication). They are also relatively common in some coasts with prevailing energetic oblique swell (Hunter et al., 1979; Guilcher et al., 1952; Pedreros et al., 1996; Lafon et al., 2002). They have been reported from both micro-tidal conditions (Falqués, 1989) and meso-tidal conditions (Lafon et al., 2002; Castelle, 2004). They can be either subtidal (Hunter et al., 1979) or intertidal (Lafon et al., 2002) referring to whether the bars are permanently covered by water or if they are alternately submerged and exposed following the tidal cycle. In the intertidal case and if they are very oblique (almost shore-parallel trending) they are also known as *ridge and runnel systems*. Some common characteristics are:

(1) They are typically attached to the shoreline at cape-like features called *mega-cusps* or giant cusps. The mega-cusps are different from the ordinary beach cusps in that the former are essentially linked to surf zone bars. Also the alongshore spacing of mega-cusps is typically one order of magnitude larger than beach cusps.
(2) Such bars very often appear as a system with a number of them located along the coast. The number can range from a few (i.e., two or three) (Konicki and Holman, 2000) to several tens (Lafon et al., 2002). The alongshore spacing λ between adjacent bars or the associated mega-cusps may be quite regular but can also display relatively large variations (for instance, 50% of the mean). In any circumstance, however, they keep the suggestion of an alongshore rhythmic system.
(3) They typically occur in intermediate beach conditions, neither in dissipative nor in reflective conditions (Wright and Short, 1984; Short, 1999).

Their growth seems to be related to post-storm conditions. Conditions favoring their existence are abundant supply of sand and very gentle slopes (Evans, 1938; Niederoda and Tanner, 1970). Oblique bar systems are often observed in beaches with oblique wave incidence, therefore coexisting with longshore currents, and they often migrate down-current at rates ranging from 0 to 10 m/day (Evans, 1939; Lafon et al., 2002; Falqués, 1989; Hunter et al., 1979). In this case, the relationship between the bar orientation and the longshore current is an open question. The 'down-current orientation', that is, the offshore end of the bar shifted down-current with respect to the shore attachment, seems to be most frequent orientation. However, the bars can orient themselves 'up-current' too (Ribas and Kroon, submitted for publication). In most cases, the hydrodynamics during the formation of the bars is however not reported from the field experiments so that the bar orientation with respect to the longshore current is not known. Even though precise flow measurements are scarce, transverse bars are associated with a cellular flow which is onshore over the bar and offshore at the adjacent troughs, with wave-focusing over the bar due to wave refraction (Niederoda and Tanner, 1970; Falqués, 1989; Short, 1999). In case of down-current oriented oblique bars, the current veers onshore over the crest of the bar and offshore at the troughs in between the bars (Evans, 1939). Some authors refer to these troughs as 'rip channels' too (Hunter et al., 1979; Castelle, 2004).

The alongshore spacing λ ranges from tens to hundreds of meters, i.e., the order of magnitude of the surf zone width, X_b. Hino (1974) reported observed spacings scattering between 3 and 8 times X_b, with a mean of $4X_b$. In analyzing several field data-sets from the literature, Falqués et al. (1996) also found a relatively constant value of $\lambda \sim 1-6X_b$. The cross-shore span of the bars is usually of the same order or smaller than the surf zone width.

2.2. Crescentic bars and rip channels

These bars have a mean trend parallel to the shore and are commonly related to a pre-existing 2D shore-parallel bar (see Fig. 3. They can display a variety of different shapes (van Enckevort, 2001; Ruessink et al., 2000; van Enckevort et al., 2004; Castelle, 2004) but the common characteristics are a structure of alternating shallower and deeper areas along the bar. The shallower sections are located onshore of the mean bar crest while the deeper areas are offshore of it. The overall shape in planview may be just a slight meandering about the mean longshore trend or the undulations may be rather pronounced, featuring an alongshore sequence of crescents with the horns (shallower parts) facing the

Table 1
Parameters for model runs

H_∞ (m)	θ_∞ (°)	$\theta_{x=250}$ (°)	T_p (s)	γ_b	d (m)
1	0°/10°	0°/6.5°	6	0.6	0.00025

H_∞ is the rms wave height and θ_∞ the incidence angle of the waves with respect to shore-normal in deep water.
The wave angle at $x=250$ m is $\theta_{x=250}$ and the sediment grain diameter is d. The peak wave period is T_p and the breaking index is γ_b.

shore. For very well developed bars, the horns may even extend up to the coastline, developing into transverse or oblique bars. Breaking waves over a crescentic bar create a circulation with onshore flow over the shallow sections and offshore flow or rip-currents over the deep sections. The latter are therefore known as rip channels. Some crescentic bars do not have a pronounced horizontal undulation but are instead characterized by a relatively straight alongshore crest cut by rip channels.

Observations of crescentic bars have been reported from many beaches around the world. In van Enckevort et al. (2004) (see Table 1 in that paper) up to 33 references on crescentic bar observations are listed, dating back to 1949. They are found in pocket beaches and also along open coasts with mean slopes less than $\beta \sim 0.05$. Crescentic bars, like transverse bars, are characteristic of intermediate beaches (Wright and Short, 1984; Lippmann and Holman, 1990; Short, 1999) and they are commonly wiped out during storms, whereas they are formed again after the peak of the storm. This behaviour has been systematically observed, for instance, at Duck (North Carolina, Atlantic USA coast), at Miyazaki (Kyushu, Japan) and at Gold Coast (Queensland, Australia) by van Enckevort et al. (2004). The destruction typically occurs for $\Omega = H_b/Tw_s \sim 7–10$ or higher, where H_b is wave height at breaking, T wave period and w_s sediment fall velocity. This parameter is an indicator of the beach morphodynamic state, low values corresponding to reflective beach conditions, high values corresponding to dissipative beach conditions (Wright and Short, 1984). The formation time is about 1–3 days. However, there are differences between different sites. In particular, the crescentic bars at Noordwijk, The Netherlands, do not show a clear pattern of generation, growth and decay, and heavy storms (even with Ω up to 20) do not lead to a total 'morphodynamic reset'. This is probably due to a morphodynamic timescale that is much longer than that of the other sites and is quite long in comparison with the time scale of weather variability. This difference in timescale could be attributed to a different tidal range, since tidal effects seem to slow down crescentic bar dynamics (Castelle, 2004), or to a mean wave period that is significantly smaller at Noordwijk (5.7 s compared with 7.3 to 9.3 at the other sites analyzed by van Enckevort et al. (2004)).

The wavelength, λ, defined as the distance between consecutive horns, ranges from several tens of meters to 2 or 3 km. In general, λ increases with distance offshore, x_c. This is very apparent for multiple bars, where the outer crescentic bar spacing is larger than that of the inner one. Values of λ/x_c reported in the literature are in the order 1–10. For instance, values observed at Duck and at Miyazaki by van Enckevort et al. (2004) during the initial formation were about 7–10. Afterwards, the spacing tended to decrease, the ratio becoming about 2–6. The term 'rhythmic' applied to crescentic bars (and also to transverse/oblique bar systems) does not mean a perfect periodicity but only a quasi-periodicity or, at least, the suggestion of some recurrent length scale along the coast. For instance, the ratio of the standard deviation in λ to its mean value along a beach can be as small as 0.05 in some cases but also as large as 0.6 in others. Also, the actual spacing after the initial formation is clearly dominated by a complex dynamics with splitting and merging of crescents as self-organized processes driven by the changes in wave conditions.

Finally, in case of shore-oblique wave incidence, crescentic bars migrate along the coast with typical celerities of tens of meters per day and, in some cases, even up to 180 m/day.

3. Morphodynamic self-organization: models

3.1. General characteristics

Nonlinear dynamical systems can exhibit complex patterns in time and space that are not related to similar patterns in the external forcing. This is known as free or self-organized behaviour. The formation of alongshore rhythmic patterns had initially been attributed to a certain *template* in the hydrodynamic forcing (Holman and Bowen, 1982). However, it is nowadays becoming more accepted that their origin is generally due to self-organized processes in the coupling between flow and morphology.

The starting point for this explanation is to assume an alongshore uniform wave forcing along with correspondingly uniform equilibrium beach morphology, so that rhythmic features are absent. Next, a perturbation of this equilibrium is considered, for instance a shoal that breaks the alongshore uniformity. This will give rise to a different flow pattern and, hence, a different sediment transport pattern. The question is then, will the new sediment transport induce deposition on or erosion of the shoal? In the former a positive feedback will occur, so that both the perturbations in the topography and in the flow will reinforce each other. In the latter case, the equilibrium will be stable and no patterns will grow 'spontaneously'. In nature, no equilibrium is exact and there are always perturbations. Formally, any perturbation can be expanded in alongshore Fourier modes. If at least one Fourier mode leads to a positive feedback between flow and morphology, the equilibrium will be unstable and a coupled pattern in the flow and the morphology corresponding to that mode will emerge in the system. This provides the explanation for many of such rhythmic bars.

Models that describe morphodynamic self-organization in the nearshore typically consist of the following elements:

(1) Wave transformation (or 'wave driver'). A description of wave refraction, shoaling, (diffraction, reflection) and breaking as they approach the coast.
(2) Mean currents and mean sea level. A description of the wave-driven mean currents over the uneven sea bed along with the mean sea level.

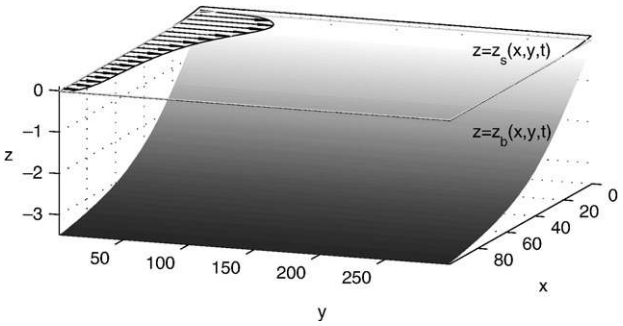

Fig. 4. Sketch of a typical integration domain of surf zone morphodynamic models. The bed level, $z=z_b(x, y, t)$, and the mean sea level, $z=z_s(x, y, t)$, are shown. The longshore current driven be obliquely incident waves is indicated.

(3) Sediment transport by currents and waves.
(4) Bed updating due to sediment conservation under gradients in sediment flux.

and they can be both linear and nonlinear (see e.g. Dodd et al., 2003):

(1) Linear models. Known more commonly as linear stability models, these are *specifically* designed to examine the aforementioned morphodynamical stability. The variables are expanded as the equilibrium quantities plus small deviations and the governing equations are then linearized with respect to the deviations (perturbations). The linearized equations are solved numerically (or analytically when it is possible) in order to find the emerging patterns and its initial growth rate.
(2) Nonlinear models. These models are not usually derived in order to examine morphodynamical instability, but in our present context arbitrary perturbations are superimposed on the equilibrium situation, which is considered as an initial condition. The fully nonlinear governing equations, or possibly a reduced set of abstracted equations, are then solved to find the time evolution of the system from those initial conditions. Thus we can discover which patterns grow and eventually prevail. The sensitivity to different initial conditions must be tested.

Among nonlinear models there are several different types, but the two most prominent are: i) those that use the basic physical laws like mass, momentum and energy conservation expressed as partial differential equations; and ii) those that use more abstract rules to formulate those physical laws. The latter are sometimes called 'cellular automata models' and have been used to study beach cusp formation (Coco et al., 2000) and shoreline instabilities (Ashton et al., 2001).

Only models based on partial differential equations have been considered for the present contribution. In such modelling a further distinction is whether the models are 'academic' or 'commercial'. The former are usually specific for the study of particular processes, and tend to be highly idealized and not user-friendly. The latter are applicable to many different scientific and technical problems (e.g., consultancy), are less idealized and more user-friendly.

3.1.1. Geometry, coordinates and variables

The different models used in this research treat different variables and different equations. We here try to present a common background for all models and later comment on particular features of each. A rectilinear and unbounded coast is considered, with Cartesian coordinate axes, x (or x_1) pointing seawards, y (or x_2) running along the coast and a vertical axis z pointing upwards (see Fig. 4). The focus is the sea bed evolution, along with the associated hydrodynamics, over a rectangular domain bounded by the coastline, an offshore boundary parallel to it, and two cross-shore sections (note, however, that if alongshore periodicity is intrinsic to the modelling approach, such as for a linear stability model, there are no lateral boundaries). The offshore boundary is far enough away so as to avoid interference with surf zone processes, i.e., well beyond the breaker line; again, however, note that this may formally be at infinity, depending on numerical methods chosen.

Since the morphological evolution is much slower than the wave-motion, waves are commonly not described individually in morphodynamic models; rather their average properties are considered. This point of view has been adopted here and the corresponding models are referred to as phase-averaged models (some comments on wave-resolving models are presented in Section 5.2). These wave properties are the absolute frequency (frequency with respect to an observer at rest), ω; the wavenumber vector, $\vec{k}(x, y, t)$; and the energy density,

$$E(x,y,t) = \frac{1}{8}\rho g H_{\mathrm{rms}}^2, \tag{1}$$

where ρ is water density and g is the gravity acceleration. Hereinafter, the vector symbol means a 2D vector in the horizontal plane (unless stated otherwise as in Section 3.4). The topographic variable is the mean bed level, $z_b(x, y, t)$. The variables pertaining to the mean hydrodynamics are the mean sea level, $z_s(x, y, t)$, and the depth and phase-averaged current (or mass flux current),

$$\vec{v}(x,y,t) = \frac{1}{D} < \int_{\tilde{z}_b}^{\tilde{z}_s} \vec{\tilde{v}}\, dz >. \tag{2}$$

The '$<\cdot>$' denotes an average over a time of the order of the wave period and $\tilde{}$ refers to instantaneous quantities, so that $z_s = <\tilde{z}_s>$, and so on. The mean water depth is therefore $D = z_s - z_b$.

3.1.2. Wave driver

To be specified for each model.

3.1.3. Mean hydrodynamics

The mean hydrodynamics is governed by the depth-averaged water mass and momentum conservation which read:

$$\frac{\partial D}{\partial t} + \frac{\partial}{\partial x_i}(D v_i) = 0 \tag{3}$$

and

$$\frac{\partial v_i}{\partial t} + v_j \frac{\partial v_i}{\partial x_j} = -g\frac{\partial z_s}{\partial x_i} - \frac{1}{\rho D}\frac{\partial}{\partial x_j}\left(S'_{ij} - S''_{ij}\right) - \frac{\tau_{bi}}{\rho D}, \quad i = 1, 2. \tag{4}$$

Hereinafter, repeated indices are assumed to be summed over $i, j = 1, 2$. In addition to the momentum input from the waves via the radiate on stress (S_{ij}) gradients, Eq. (4) includes momentum dissipation through the lateral mixing from the turbulent Reynolds stresses, S''_{ij}, and through the bed shear stresses, $\vec{\tau}_b$. These three quantities will be specified for each model.

3.1.4. Sediment transport

To be specified for each model.

3.1.5. Bed updating

The system of governing equations is closed with the bed updating equation, which describes sediment conservation:

$$\frac{\partial z_b}{\partial t} + \frac{1}{1-n}\frac{\partial q_i}{\partial x_i} = 0 \tag{5}$$

where $\vec{q}$ is the vertically averaged sediment flux ($m^2\ s^{-1}$) and n is the porosity of the seabed. The models we are describing consider a single sediment grain size.

3.2. Morfo60

MORFO60 (Calvete et al., 2002, 2005) is a linear stability model specifically designed to study both hydrodynamic or morphodynamic instabilities of an alongshore uniform coast. As such it may describe any alongshore periodic small amplitude water motion as edge waves or shear waves but it is here applied to study the generation of alongshore rhythmic topography.

3.2.1. Formulation and governing equations

For the wave driver, the waves are assumed linear and Rayleigh distributed in height but monochromatic, with a single absolute frequency ω and a single incidence angle θ. Wave energy is governed by

$$\frac{\partial E}{\partial t} + \frac{\partial}{\partial x_i}\left(\left(v_i + c_{gi}\right)E\right) + S'_{ij}\frac{\partial v_j}{\partial x_i} = -\mathcal{D} \tag{6}$$

where

$$S'_{ij} = E\left(\frac{c_g}{c}\frac{k_i k_j}{k^2} + \left(\frac{c_g}{c} - \frac{1}{2}\right)\partial_{ij}\right) \tag{7}$$

is the wave radiation stress, c, c_g are the phase and group celerities, and δ_{ij} is the Kronecker delta. The wave-breaking dissipation, $\mathcal{D}$, is formulated following Church and Thornton (1993) for irregular waves. Wave propagation is described by the geometric optics approximation with a phase function $\phi(x, y, t)$ such that $\partial\phi/\partial t = -\omega$ and $\vec{\nabla}\,\phi = \vec{k}$ and whose governing equation is:

$$\frac{\partial \phi}{\partial t} + \hat{\omega} + v_i\frac{\partial \phi}{\partial x_i} = 0, \tag{8}$$

where $\hat{\omega} = \sqrt{gk\tanh kD}$ is the intrinsic frequency, the one with respect to an observer moving with the current. Note that Eqs. (6,8) take wave–current interactions and refraction into account, but not diffraction or reflection of the waves.

Regarding the parameterizations in the momentum equations, Eq. (4), the Battjes (1975) formulation is used according to which

$$S''_{ij} = \rho \nu_t D\left(\frac{\partial v_i}{\partial x_i} + \frac{\partial v_j}{\partial x_i}\right) \quad , \quad \nu_t = M\left(\frac{\mathcal{D}}{\rho}\right)^{\frac{1}{3}} H_{\mathrm{rms}}, \tag{9}$$

with a constant mixing coefficient $M=1$. The bed shear stress is described by a linear friction law with a depth dependent drag coefficient:

$$\vec{\tau}_b = \rho c_d (2/\pi) u_{\mathrm{rms}} \vec{v} \quad , \quad c_d = \left[\frac{0.40}{\ln(D/z_0) - 1}\right]^2. \tag{10}$$

where u_{rms} is the mean-square wave orbital velocity at the boundary layer edge (Calvete et al., 2005).

For the sediment transport, a total load formulation where the volumetric sediment transport flux, $\vec{q}$ is expressed as

$$\vec{q} = \alpha\left(\vec{v} - \gamma u_{\mathrm{rms}} \vec{\nabla} h\right) \tag{11}$$

where $h(x, y, t)=z_b(x, y, t)-z_b^0(x)$ is the bed level perturbation with respect to the equilibrium beach profile and where the stirring function is taken from the formulation of Soulsby–Van Rijn (Soulsby, 1997):

$$\alpha = A_s\left[\left(|\vec{v}|^2 + \frac{0.018}{c_d} u_{\mathrm{rms}}^2\right)^{1/2} - u_{\mathrm{crit}}\right]^{2.4} \tag{12}$$

Here, the factor A_s depends on sediment properties and water depth and the constant γ is set to $\gamma=5$ (both for MORFO60 and MORFO55). In this sediment transport formulation the sediment is stirred by the combined effect of currents and waves, and is advected by the current. The Soulsby–Van Rijn formula (Eqs. 11 and 12) is intended for conditions in which the bed is rippled (Soulsby, 1997). Thus, it should be used with caution in other cases. On barred beaches, under moderate to large wave energies, sheet flow conditions are often found over the bar and at the swash, whereas bed ripples are found at the shoreface and in the trough behind the bar. For the present applications, it is assumed that within the surf zone the bed regime corresponds mainly to rippled bed, which is valid under weak to moderate wave conditions.

Note that the current in Eqs. (11,12) is depth-averaged, so undertow is not accounted for. Likewise, the onshore transport due to wave asymmetry is not included. The rationale for this is that the latter transport together with the undertow and downslope transport associated with the equilibrium slope, dz_b^0/dx, are approximately in balance to build the equilibrium profile. When the alongshore uniform equilibrium is broken, it is assumed that those terms are still approximately in balance and that there is only a need for describing the sediment transport driven by the longshore current and rip-currents together with the perturbation in downslope transport, Eq. (11). This simplification is supported by the experimental observation that even relatively small alongshore bathymetric inhomogeneities drive strong currents (rip-currents, for instance). These currents overwhelm the possible unbalance in the wave-driven cross-shore transport, especially for intermediate beach states, which is the situation where rhythmic topography typically occurs.

Thus, the sets of Eqs. (3–6, 8), comprise a system to be solved for the six unknowns $E(x, y, t)$, $\phi(x, y, t)$, $z_s(x, y, t)$, $\vec{v}(x, y, t)$ and $z_b(x, y, t)$.

3.2.2. Stability problem

First, an equilibrium beach profile, $z_b=z_b^0(x)$ is prescribed. Since the wave-driven cross-shore sediment transport is not explicitly included, it can be chosen arbitrarily. We then seek a steady and alongshore uniform solution of Eqs. (4–6), (Eq. 5 being automatically satisfied):

$$E = E_0(x),\ \phi = \varphi(x) + yk_y - \omega t,\ z_s = z_s^0(x),\ \vec{v} = (0, V(x)) \tag{13}$$

for k_y=constant (implying once more alongshore uniformity). Note that $\phi=\phi(x, y, t)$ is not steady and not necessarily alongshore uniform but ω and $\vec{k}$ are. This provides the basic equilibrium solution.

Once the basic state is found, all the variables are expanded as equilibrium quantities plus perturbations, i.e.,

$$\begin{aligned} &E = E_0(x) + E'(x,y,t), \quad \phi = \phi_0(x,y,t) + \phi'(x,y,t) \\ &z_s = z_s^0(x) + \eta(x,y,t), \quad \vec{v} = (0, V(x)) + \vec{v}', \quad z_b = z_b^0(x) + h(x,y,t). \end{aligned} \tag{14}$$

After inserting these expansions, Eqs. (3–5) together with (6) and (8) are linearized with respect to the perturbations E', ϕ', η, $\vec{v}'$, h. The resulting equations are linear with coefficients that do not depend on t and y. Therefore, the solutions may be found in the form

$$\left\{E', \phi', \eta, v_x', v_y', h\right\} = e^{\sigma t + iKy}\left\{\hat{E}(x), \hat{\phi}(x), \hat{\eta}(x), \hat{v}_x(x), \hat{v}_y(x), \hat{h}(x)\right\} \tag{15}$$

and, inserting this ansatz in the linearized equations, a system of ordinary differential equations results, which is an eigenproblem where a is the eigenvalue and ($\hat{E}(x)$, $\hat{\phi}(x)$, $\hat{\eta}(x)$, $\hat{v}_x(x)$, $\hat{v}_y(x)$, $\hat{h}(x)$) are the eigenfunctions. The eigenproblem is solved by numerical spectral methods in the semi-infinite domain $0<x<\infty$ with the boundary condition that all the perturbations vanish as $x\to\infty$. A fixed small vertical wall is assumed at the shoreline and consistent boundary conditions are assumed there. For each alongshore wavenumber K a spectrum of eigenvalues a with corresponding eigenvectors ($\hat{E}(x)$, $\hat{\phi}(x)$, $\hat{\eta}(x)$, $\hat{v}_x(x)$, $\hat{v}_y(x)$, $\hat{h}(x)$) is found. In general, a is complex and its real part, $\Re e(\sigma)$ gives the growth rate and its imaginary part gives the alongshore migration celerity, $V_{mi}=-\Im m(\sigma)/K$. The eigenvector provides the cross-shore structure of the solutions and $\lambda=2\pi/K$ its alongshore periodicity (alongshore spacing of the rhythmic features). The emerging patterns correspond to solutions with $\Re e(\sigma)>0$ and the characteristic growth time is given by the e-folding time, $(\Re e(\sigma))^{-1}$.

3.3. Morfo55

This nonlinear model is an extension of the earlier MORFO50 described in Caballeria et al. (2002). It shares with MORFO60, the governing equations coming from the mean hydrodynamics, sediment transport and bed updating, Eqs. 3, 4 and 5, for the unknowns $z_s(x, y, t)$, $\vec{v}(x, y, t)$ and $z_b(x, y, t)$. The same turbulent momentum mixing formulation, Eq. 9, is used. For the bed shear stress due to waves and current, an average over time and the Rayleigh distribution is taken, giving

$$\vec{\tau}_b = \rho c_d |\vec{v}|\vec{v} + \rho\frac{c_d}{\sqrt{\pi}}\frac{u_{\rm rms}\vec{v}}{1+1.6\hat{v}+2.5\hat{v}^2} + \rho\frac{c_d}{\sqrt{\pi}}\frac{\left(u_{\rm rms}|\vec{v}|+|\vec{v}|^2\right)\cos\Psi}{1.081-0.043\Psi+(0.351+0.55\Psi)\hat{v}+(1.26-0.098)\Psi)\hat{v}^2}\frac{\vec{k}}{k}, \tag{16}$$

where Ψ is the angle between $\vec{k}$ and $\vec{v}$(in rad.), $\hat{v}=|\vec{v}|/u_{\rm rms}$ and c_d is a constant drag coefficient.

Regarding the wave driver, there are several options:

(1) Geometric optics approximation as in MORFO60. Then Eqs. 6 and 8 are considered for the unknowns $E(x, y, t)$ and $\phi(x, y, t)$.
(2) Snell's law as an approximation to compute wave direction, which is good in the limit of very large alongshore spacing. Consistently with this, wave–current interaction is not included. The wave energy $E(x, y, t)$ is computed by using Eq. 6 and the phase is obviously not needed in this option.
(3) External, based on the REF/DIF model (Kirby and Dalrymple, 1994) which uses the parabolic approximation of the mild-slope equation, accounting mainly for refraction, diffraction, and wave breaking.

The second option has been used to obtain the results presented here.

MORFO55 can use various parameterizations of sediment transport, but the application presented here has been made by using the sediment flux Eq. 11 with the aforementioned Soulsby–Van Rijn parameterization.

The computational domain is a rectangle bounded by the shoreline, $x=0$, an offshore boundary, $x=L_x$, and two cross-shore sections, $y=0$ and $y=L_y$. The boundary conditions are the same as Caballeria et al. (2002). The shoreline is defined as a small wall, which is not allowed to move. Given the initial conditions for the bathymetry and the flow, the system of the fully nonlinear equations is integrated numerically to determine the time development of topographic features with the associated hydrodynamics. The integration is performed by finite differences (on a staggered grid) in space and by an explicit Adams–Bashforth scheme in time (see Caballeria et al. (2002) for the details). Further information on this model may be found in Garnier et al. (2006).

3.4. LFW-2d

This is a nonlinear model which solves for the surf zone hydrodynamics over a given and fixed bed topography, $z=z_b(x, y)$. Thus, sediment transport and bed updating are not considered. A moving shoreline is the most important feature of this model. The variables are the depth-averaged current, $\vec{v}(x, y, t)$, water depth, $D(x, y, t)=z_s-z_b$, wave energy, $E(x, y, t)$ and wavenumber, $\vec{k}(x, y, t)$.

In order to pursue a robust modelling approach allowing realistic bathymetries and a moving shoreline, a flux-conservative, finite volume approach is taken. The model equations are therefore written in an appropriate form. The water mass conservation is exactly as Eq. 3 and the momentum equations, Eq. 4, are written in a slightly different way to allow for the vector form, Eq. 20. The bed shear stress is taken as

$$\vec{\tau}_b = \rho c_d |\vec{v}|\vec{v} \tag{17}$$

where c_d is a constant drag coefficient. The turbulent momentum mixing is similar to MORFO60 and MORFO55.

The wave energy transformation, including shoaling on currents, is written in terms of the wave action, $\varepsilon = E/\hat{\omega}$, as

$$\frac{\partial \varepsilon}{\partial t} + \frac{\partial}{\partial x_i}\left(\left(v_i + c_{gi}\right)\varepsilon\right) = -\frac{\mathcal{D}}{\hat{\omega}}. \tag{18}$$

Wave refraction (on depth and currents) is formulated as

$$\frac{\partial k_i}{\partial t} + \frac{\partial}{\partial x_j}\left[\left(v_j + c_{gj}\right)k_i\right] = k_i \frac{\partial c_{gj}}{\partial x_j} - \frac{\partial\, \hat{\omega}}{\partial D}\frac{\partial D}{\partial x_i} + (-1)^{3-j} k_j \frac{\partial v_{3-i}}{\partial x_{3-j}}. \tag{19}$$

Then, the governing equations are written in vector form as:

$$\frac{\partial \vec{W}}{\partial t} + \frac{\partial \vec{F_j}}{\partial x_j} = \vec{S} \tag{20}$$

where

$$\vec{W} = [D, Dv_1, Dv_2, \varepsilon, k_1, k_2]^T \tag{21}$$

$$\vec{F_1} = \left[Dv_1, Dv_1^2 + \frac{1}{2}gD^2, Dv_1v_2, \left(v_1 + c_{g1}\right)\varepsilon, \left(v_1 + c_{g1}\right)k_1, \left(v_1 + c_{g1}\right)k_2\right]^T \tag{22}$$

$$\vec{F_2} = \left[Dv_2, Dv_1v_2, Dv_2^2 + \frac{1}{2}gD^2, \left(v_2 + c_{g2}\right)\varepsilon, \left(v_2 + c_{g2}\right)k_1, \left(v_2 + c_{g2}\right)k_2\right]^T \tag{23}$$

$$\begin{aligned}\vec{S} = \Bigg[0, -gD\frac{\partial z_b}{\partial x_1} - c_d v_1|\vec{v}| - \frac{\partial S'_{11}}{\partial x_1} - \frac{\partial S'_{12}}{\partial x_2} + \frac{\partial S'_{11}}{\partial x_1} + \frac{\partial S''_{12}}{\partial x_2}, -gD\frac{\partial z_b}{\partial x_2} - c_d v_2|\vec{v}| - \frac{\partial S'_{21}}{\partial x_1} - \frac{\partial S'_{22}}{\partial x_2} + \frac{\partial S''_{21}}{\partial x_1} + \frac{\partial S''_{22}}{\partial x_2},\\ -\frac{\mathcal{D}}{\hat{\omega}}, k_1\frac{\partial c_{g1}}{\partial x_1} + k_1\frac{\partial c_{g2}}{\partial x_2} + k_1\frac{\partial v_2}{\partial x_2} - k_2\frac{\partial v_2}{\partial x_1} - \frac{\partial\, \hat{\omega}}{\partial D}\frac{\partial D}{\partial x_1}, k_2\frac{\partial c_{g1}}{\partial x_1} + k_2\frac{\partial c_{g2}}{\partial x_2} + k_2\frac{\partial v_1}{\partial x_1} - k_1\frac{\partial v_1}{\partial x_2} - \frac{\partial\, \hat{\omega}}{\partial D}\frac{\partial D}{\partial x_2}\Bigg]^T\end{aligned} \tag{24}$$

with $\vec{v} = (v_1, v_2)$. For simplicity ρ is here factored out from the radiation and turbulent stresses.

This hyperbolic system is solved using an explicit, second order, shock-capturing scheme, which can be written as

$$\vec{W}^{n+1}_{p,q} = \vec{W}^{n}_{p,q} - \frac{\Delta t}{\Delta x}\left(\vec{F}^{n}_{1;p+\frac{1}{2},q} - \vec{F}^{n}_{1;p-\frac{1}{2},q}\right) - \frac{\Delta t}{\Delta y}\left(\vec{F}^{n}_{2;p,q+\frac{1}{2}} - \vec{F}^{n}_{2;p,q-\frac{1}{2}}\right) + \Delta t\, \vec{S}^{n}_{p,q} \tag{25}$$

where, e.g. $\vec{W}^{n}_{p,q} = \vec{W}\,(p\Delta x, q\Delta y, n\Delta t)$. Δx (Δy) are cross-shore (alongshore) cell edge lengths on a Cartesian grid, and Δt is a time-step. Simulations are driven from the offshore boundary in terms of a wave envelope, which itself drives (depth-uniform) currents, and the offshore boundary is also absorbing to outgoing waves. Lateral boundaries can either be periodic or absorbing, although the arbitrary depth allowed at lateral boundaries necessitates a crude, first order absorbing boundary condition there.

The fluxes between cells are approximated using local Riemann solutions (see e.g. Toro, 1997). These are evaluated using Roe's approximate Riemann solver, in which the Jacobian matrices $\partial\vec{F_i}/\partial\vec{W}$ are calculated. The source terms are all treated in a pointwise fashion, apart form the bedslope terms in the momentum equations, which are upwinded (see Hubbard and Garcia-Navarro, 2000). For computations here $k_d = 0.0025$. The approach allows for a moving shoreline with wetting and drying, based on a minimum wet cell depth (here $D_{\min} = 1.0$ mm). This is atypical in a phase-averaged model, but is desirable not least because it allows shoreline movements due to groupiness and low-frequency waves to be simulated. Other model extensions are under way.

3.5. M-shorecirc

The M-SHORECIRC model (Fachin and Sancho, 2004a) is also a nonlinear process-based morphodynamic model, which solves the conservation laws of mass and momentum for the hydrodynamics, and the sediment conservation equation for the seabed. It is built upon the nearshore circulation model SHORECIRC (Van Dongeren et al., 1994; Svendsen et al., 2001), extended by means of a morphological module.

The mean hydrodynamics is governed by mass and momentum conservation, Eqs. 3 and 4 in conservative form. The details of bottom shear stress description may be seen in the references above and Sancho (1998). It is worth mentioning that this model includes the effects of both the wave radiation stresses and wave volume flux. The latter represents the wave-averaged contribution of the volume of water that crosses a section between the bottom and wave crest. For linear waves this volume of water is non-zero due to differences between crest and trough elevations. The wave radiation stresses S'_{ij} and wave volume fluxes Q_{wi} are calculated from

linear wave theory for all points within the domain (Eq. (7)). Inside the surf zone, an extra contribution is added as a result of the roller (Svendsen, 1984).

The SHORECIRC model can also account for vertically-varying currents, through an analytical solution for the current profiles (Putrevu and Svendsen, 1999). As our goal is to describe slowly-varying topographies of nearly longshore-uniform coasts, under those conditions the longshore currents are essentially depth-uniform (Sancho, 1998). Despite the cross-shore currents within the wave-breaking region having a strong depth variation, several sediment transport formulas use depth-averaged currents. Thus, we use here, in SHORECIRC, the depth-uniform approximation for the horizontal currents, as in the other models described earlier.

The wave field in SHORECIRC is computed by means of an external short-wave model, coupled to the wave-averaged hydrodynamic model. The present version includes the REF/DIF model (see Sec. 3.3). Wave–current interaction is an option in the SHORECIRC model, but since this effect is minor in the present applications, this option was turned off.

The sediment flux is presently computed by a similar form of the sediment flux relation of Soulsby–Van Rijn Eq. 11, but with the downslope gravitational term applied to the instantaneous bed level $z_b(x, y, t)$, instead of the perturbation $h(x, y, t)$. Furthermore, we assume the sediment flux vector aligned with the (wave-averaged) current.

In the sediment transport calculations, the depth-averaged cross-shore current v_x is replaced by the mean undertow U estimated as follows. For a long straight coast under uniform wave conditions, the wave and depth-averaged steady cross-shore current is null, in order to satisfy the mass conservation Eq. 3. That means that the integrated return current under the wave-trough equals the (non-zero) wave-averaged volume flux transported by the waves, above the wave-trough. Assuming the below-trough currents to be uniform along the vertical, a simple undertow current U, is estimated as the wave-induced volume flux Q_{wx}, divided by the local depth D, $U=Q_{wx}/D$.

The M-SHORECIRC solves the governing equations for the unknowns $z_s(x, y, t)$, $\vec{v}(x, y, t)$, $z_b(x, y, t)$, $E(x, y, t)$ and $\phi(x, y, t)$ over a rectangular grid, using finite difference methods. Actually, $E(x, y, t)$ and $\phi(x, y, t)$ are decoupled from the rest and are evaluated by the external wave driver.

The hydrodynamics and morphodynamics are updated at different time-steps. A new wave field is also computed at every morphological time-step. The ratio of the morphological to the hydrodynamical time-step is of order 10.

3.6. LEGI model

The model is based on the commercial model TELEMAC, which simulates the depth-averaged mean hydrodynamics forced by the wave radiation stresses and the tides (LNHE-Chatou, 2002b). The model solves Eqs. 3 and 4 with a tidal and Coriolis forcings which are here turned off.

The wave description is made by means of a hyperbolic rewriting of the elliptic extended mild-slope equation (see e.g. Lee et al., 1998).

Sediment transport and bed evolution is carried out with the SISYPHE (LNHE-Chatou, 2002a) sand transport module which solves Eq. 5. The total load sediment transport formula of Bijker (1968) based on the total depth-averaged current $\vec{v}$ and the wave orbital velocity is considered. It reads as Eq. 11 with $\gamma=0$ and

$$\alpha = a\exp(-0.27(\rho_s - \rho)gd/\tau_{cw}) \tag{26}$$

where a is a constant, ρ is the sediment density and τ_c, τ_{cw} are the bed shear stresses under current and under current and waves, respectively. The latter is given by

$$\tau_{\mathrm{cw}} = \quad 1 + b\left(\frac{u_{\mathrm{rms}}}{|\vec{v}|}\right)^2\tau_c \tag{27}$$

b being a constant if $|\vec{v}|\neq 0$ or

$$\tau_{\mathrm{cw}} = \frac{1}{4}\rho f_w u_{\mathrm{rms}}^2 \tag{28}$$

otherwise, with f_w being the friction factor while

$$\tau_c = \frac{1}{2}\rho f_c|\vec{v}|^2 \tag{29}$$

where f_c is the friction factor for the current.

The time stepping assumes a quasi-steady approach for the mean hydrodynamics and the wave field, i.e., the wave field and the currents are assumed to be steady and in equilibrium with the slowly evolving topography. Thus, at each morphological time-step (time-step at which the sea bed is updated) the wave-driven currents are allowed to reach an equilibrium state before using them for the new bed updating. The entire process is repeated on a basis of the new sea bed bathymetry. This is different from MORFO55 and

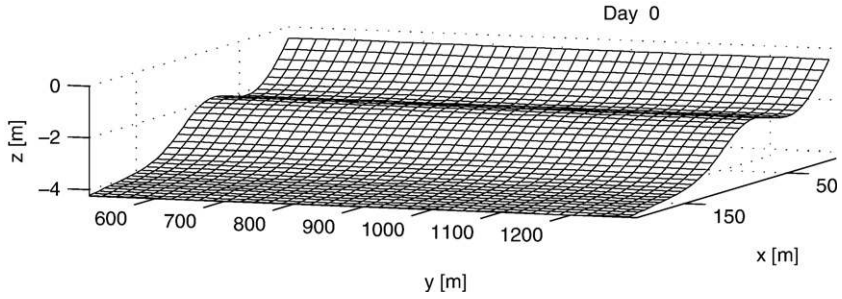

Fig. 5. 3D view of the initial bathymetry for the application of the models.

M-SHORECIRC where the unsteady hydrodynamics is computed simultaneously to the bed evolution. Good results are obtained from a comparison against data (Larroudé and Camenen, 2004).

The spatial discretization is based on a finite element method. Regarding the initial bottom perturbations there are several options, including the option of taking them from the output of a linear stability model (Ribas et al., 2003).

4. Model applications

The models described in the last section were developed (or partly developed) within the HUMOR project by various research teams and were applied by them to several problems within the morphodynamics of surf zone rhythmic features. In particular, MORFO60 was applied to a systematic study of crescentic bar formation (Calvete et al., 2005) and MORFO55 has been applied to the investigation of the finite amplitude dynamics of transverse and oblique bars on a planar beach (Garnier et al., 2006). Furthermore, both the generation of oblique bars and crescentic bars have been investigated with M-SHORECIRC (Fachin and Sancho, 2004a,b). Consistently with the aim of the present paper we do not go into the details of those problems and now focus on a comparison of the different models by applying them to a common test case.

To this end, an alongshore uniform beach profile featuring a shore-parallel bar at a distance of 80 m from the coastline is considered (see Figs. 5 and 11). The analytical profile used by Yu and Slinn (2003) to approximate the barred beach profile measured at Duck, North Carolina has been chosen. It reads

$$z_b^0(x) = a_0 - a_1\left(1-\frac{\beta_2}{\beta_1}\right)\tanh\left(\frac{\beta_1 x}{a_1}\right) - \beta_2 x + a_2\exp\left[-5\left(\frac{x-x_c}{x_c}\right)^2\right] \quad (30)$$

where $x=0$ is the still water shoreline, $x_c=80$ m is the bar location and $a_2=1.5$ m is the bar amplitude. The other parameter is fixed to $a_1=2.97$ m and the shoreline and offshore slopes are $\beta_1=0.075$ and $\beta_2=0.0064$. The integration domain is a the rectangle defined by $0<x<250$ m and $0<y<2000$ m. Parameter a_0 indicates the minimum water depth that the model is resolving, which is representative of the offshore boundary of the swash zone.

Single grain size of $d=0.25$ mm is considered. Waves of $H_{\mathrm{rms}}=1$ m and $T_p=6$ s are assumed to arrive at the coast either normally, $\theta_\infty=0$ (case 1), or with an angle $\theta_\infty=10°$ with the shore-normal in deep water (case 2). In both situations, the alongshore uniform bathymetry is expected to be unstable and a crescentic shape along with rip channels are expected to form if small irregularities are added in top of the basic beach profile. This is tested with MORFO55 and LEGI model. To test the robustness of the circulation associated to the formation of the crescentic shape and, in particular, the possible influence of the moving shoreline, the hydrodynamical LFW-2d model is applied on the 'final' bathymetry of those models. Prior to all this, a prediction of the initially emerging pattern and its growth rate is made by using the linear stability model MORFO60. A summary of parameter values for model runs is presented in Table 1.

4.1. Normal wave incidence

4.1.1. Morfo60

The MORFO60 model has been run for the parameter set described in Table 1. First the basic alongshore uniform state has been found (this is illustrated in Fig. 11 for the case of

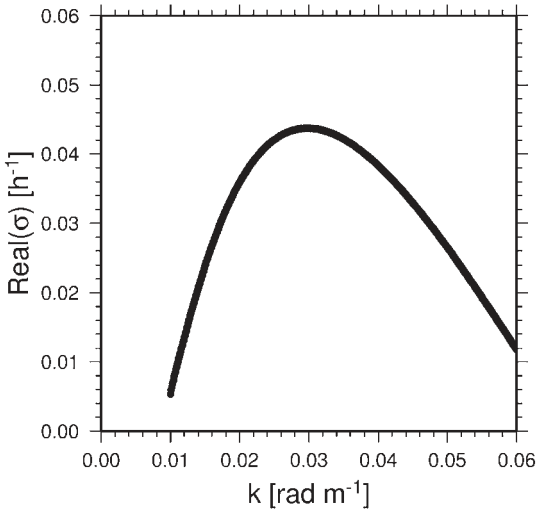

Fig. 6. Growth rate $\Re e(\sigma)$ versus wavenumber, K, for the crescentic bar obtained with MORFO60 in case of normal wave incidence.

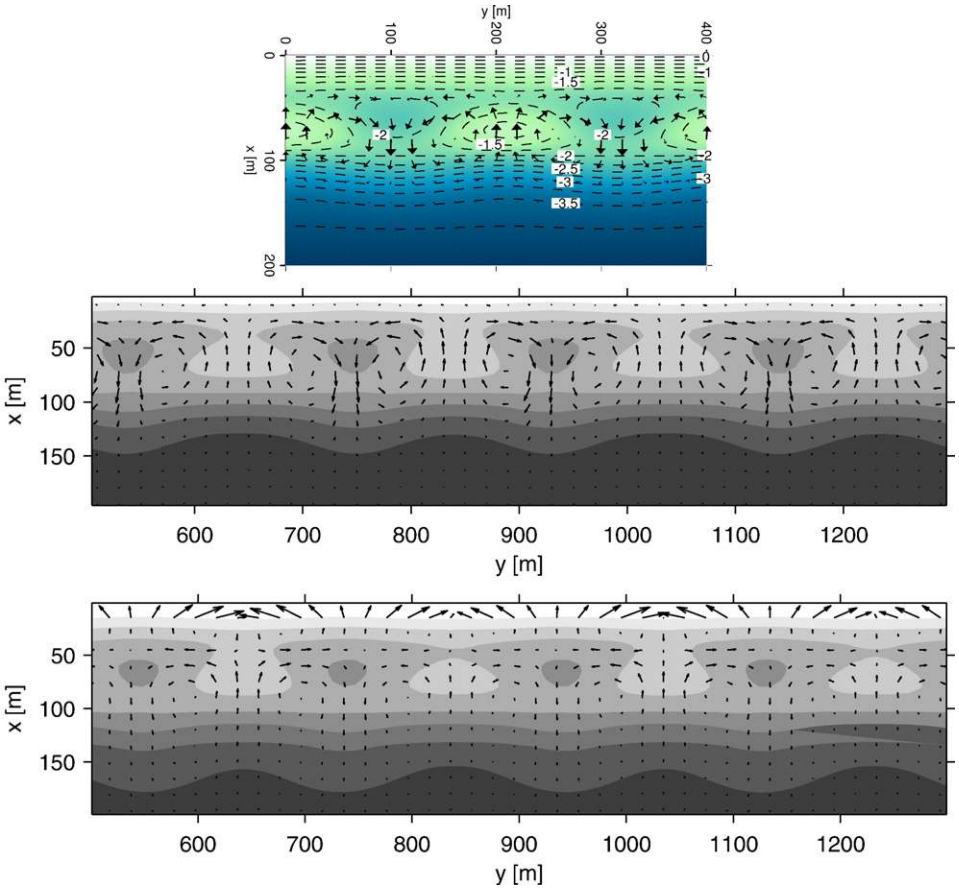

Fig. 7. Bathymetry and circulation emerging from the morphodynamic instability of the barred profile given by Eq. 30 for shore-normal wave incidence. Top: Linear stability prediction with MORFO60. The amplitude of the bathymetric perturbation has arbitrarily been chosen as 0.5 m. The maximum current intensity is then 0.44 m^{-1}. Middle: bathymetry and current after 100 d of morphological evolution computed with MORFO55. The maximum current intensity is 0.32 m s^{-1}. Bottom: Circulation on the final bathymetry of MORFO55 computed with LFW-2d. The maximum current intensity is 0.52 m s^{-1}.

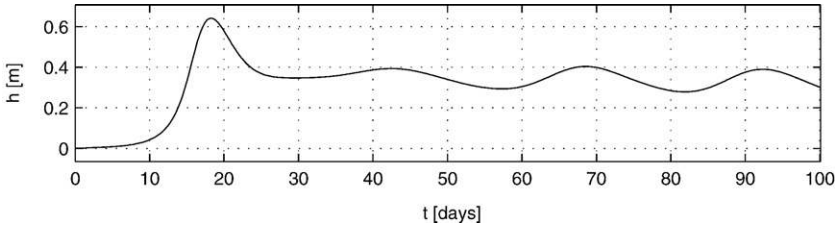

Fig. 8. Time evolution of bed level (difference with respect to initial value) at point $x=50$, $y=1000$ m computed with MORFO55 for normal wave incidence.

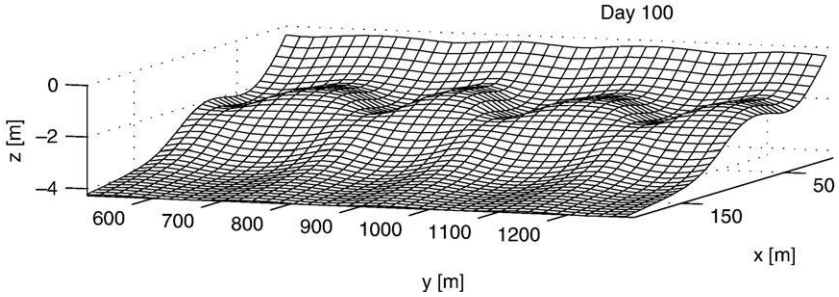

Fig. 9. 3D view of the bathymetry after 100 d of morphological evolution with MORFO55 in case of normal wave incidence.

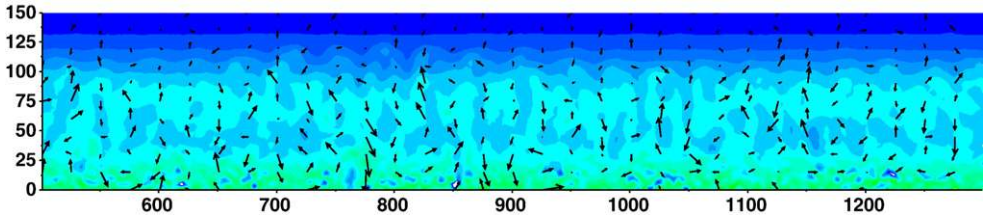

Fig. 10. Bathymetry and circulation after 100 d of morphological evolution computed with the LEGI model for shore-normal wave incidence. Maximum current intensity: 0.4 m s^{-1}.

oblique wave incidence). Then, the linear stability analysis has been performed for a range of alongshore wavenumbers K which are relevant for the expected spacing of rip channels. For each K the spectrum of a values is obtained many of them being not physically relevant. It is not trivial how to select them and extensive discussion of the procedure for it can be found in the literature on linear stability analysis in coastal morphodynamics (see, e.g., Falqués et al. (2000); Ribas et al. (2003); Calvete et al. (2005) and references herein). After selecting the relevant mode (here a crescentic bar mode), the $\Re e(\sigma)$ diagram as a function of K is plotted as shown in Fig. 6. A maximum is clearly seen, indicating a fastest growing (i.e., dominant) wavenumber which corresponds to a rip spacing $\lambda=211$ m. The associated e-folding time of the growth is $(\Re e(\sigma))^{-1}=23$ h. Fig. 7 shows the corresponding spatial pattern in the bathymetry and in the mean current. As the linear stability does not give information on the amplitude of the emerging pattern, an amplitude of $A=0.5$ m has been assumed for the plot in order to reproduce a total bathymetry (basic+perturbation) to be compared with the outputs of the nonlinear models. For this amplitude, the maximum intensity of the rip-current circulation is $u=0.44$ m s^{-1}. In agreement with what is observed in nature, the current is offshore directed at the channels and onshore directed at the shoals between the channels.

4.1.2. Morfo55

The time evolution up to $t=100$ d of the bathymetry and the mean current has been computed with MORFO55 starting from the initial bathymetry shown in Fig. 5 plus small perturbations (amplitude of about 0:03 m). The friction coefficient is set to $c_d=0.01$. Fig. 8 shows the evolution of the bed level at a point in the middle of the domain ($x=50$, $y=1000$ m). It is seen that the bed level at this point keeps on rising during some 20 d and after a maximum increase of $h=0.65$ m with respect to its initial value, it decreases and starts to oscillate around $h=0.35$ m. The initial amplification period of 20 d is much longer than the e-folding time obtained with MORFO60, which is about 1 d. For numerical reasons the initial perturbations have been taken very small. Therefore, it takes a long time to reach a significant amplitude of the crescentic shape. However, the e-folding time can be evaluated from the initial growth in Fig. 8 estimating the time needed to amplify the amplitude, e.g. in time $t=10$ d, by a factor e. This gives an e-folding time of about 2 d.

The bathymetry at $t=100$ d is shown in Figs. 7 and 9. The former also shows the circulation. It is seen that the initially straight bar has become crescentic and features rip channels with an alongshore spacing of about $\lambda=200$ m. The amplitude of the bathymetric perturbation, i.e., half the maximum bed level difference between shoals and channels is $A=0.53$ m. In qualitative agreement with MORFO60 instability mode (and with observations), the current is offshore directed at the channels and onshore

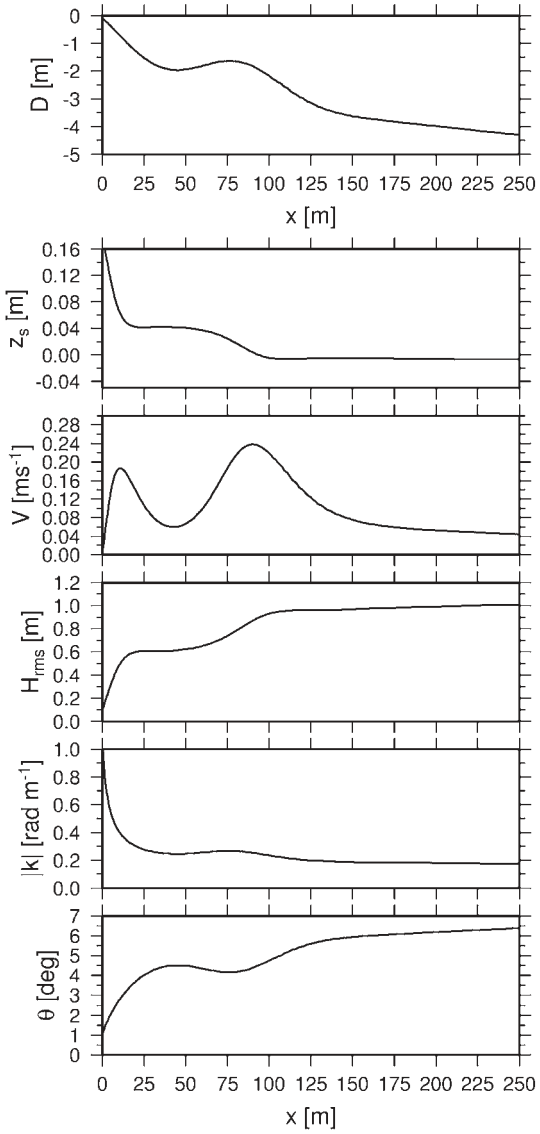

Fig. 11. Alongshore uniform basic state in case of oblique wave incidence obtained with the basic state module of MORFO60. From top to bottom: bathymetry, mean sea surface level, longshore current, wave height, wavenumber and wave incidence angle.

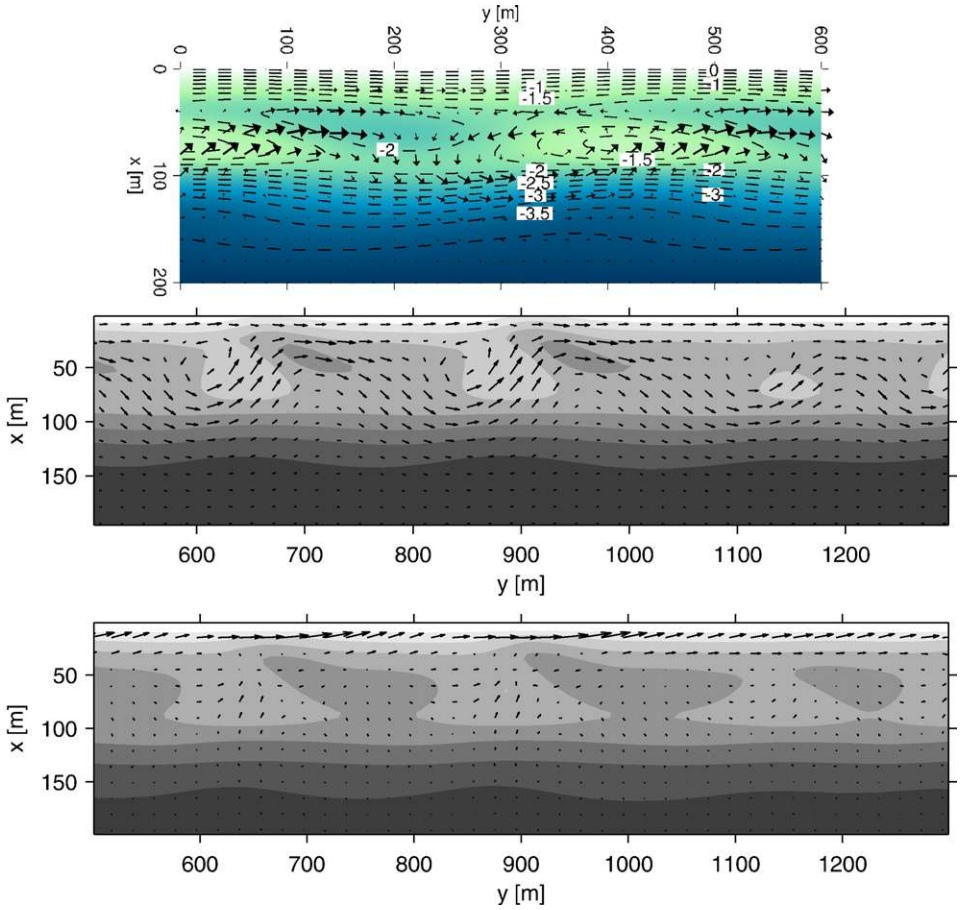

Fig. 12. Bathymetry and circulation emerging from the morphodynamic instability of the barred profile given by Eq. 30 for oblique wave incidence. Top: Linear stability prediction with MORFO60. The amplitude of the bathymetric perturbation has arbitrarily been chosen as 0.5 m. The maximum current intensity is then 0.5 m^{-1}. Middle: bathymetry and current after 100 d of morphological evolution computed with MORFO55. The maximum current intensity is 0.42 m^{-1}. Bottom: Circulation on the final bathymetry of MORFO55 computed with LFW-2d. The maximum current intensity is 1.06 m s^{-1}.

directed at the shoals between the channels. The maximum current intensity is in the rips and is about 0.32 m s^{-1}.

4.1.3. LEGI model

Surprisingly, the LEGI model does not predict the formation of a crescentic bar for the same initial bathymetry and the same wave conditions. As displayed in Fig. 10, a quite irregular bathymetry is obtained after 100 d of wave action. The trough between the shoreline and the bar has been partly replenished and the bar-trough system has become a terraced beach. Some alongshore rhythmicity (rather irregular) is apparent in small channels and undulations in the contour lines somewhat offshore of the bar. The circulation is quite irregular too, featuring small vortices and with a maximum current intensity of 0.4 m s^{-1}.

4.1.4. LFW-2d

The purely hydrodynamic LWF-2d model has been run over the final bathymetry obtained with MORFO55 for normal wave incidence as it is illustrated in Fig. 7. Around the location of the longshore bar the circulation is qualitatively similar even with a similar maximum current intensity of about 0.35 m s^{-1}. The most prominent difference in this area is that in contrast with MORFO55 the rip-currents are now not stronger than the onshore return current. But the most important difference is that LWF-2d predicts secondary counter-rotating circulation cells

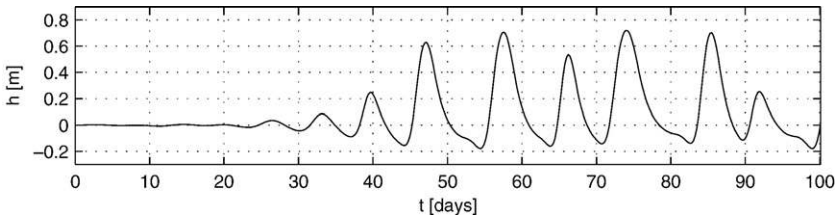

Fig. 13. Time evolution of bed level (difference with respect to initial value) at point $x=50$, $y=1000$ m computed with MORFO55 for oblique wave incidence.

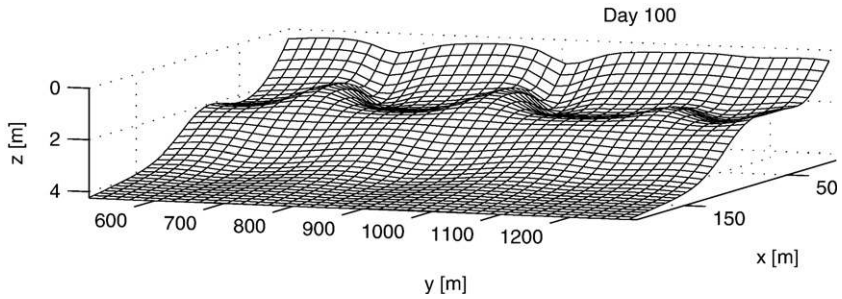

Fig. 14. 3D view of the bathymetry after 100 d of morphological evolution with MORFO55 in case of oblique wave incidence.

next to the shoreline and the maximum current intensity, 0.52 m s^{-1}, is found within these cells. It is interesting to note that these cells had been observed in purely hydrodynamic simulations (see Yu and Slinn, 2003) just forced by the bathymetric undulations over the bar crest without any bathymetric perturbation onshore of the bar.

4.2. Oblique wave incidence

4.2.1. Morfo60

The MORFO60 model has been run for a deep water wave angle $\theta_\infty = 10°$. The basic alongshore uniform state is shown in Fig. 11. Again, the linear stability analysis has been performed for the range of relevant alongshore wavenumbers K. A maximum growth rate for the crescentic bar mode is now found for a wavelength $\lambda = 411$ m and an e-folding time of $(\Re e(\sigma))^{-1} = 100$ h. This spatial pattern is shown in Fig. 12 again assuming an amplitude of $A = 0.5$ m. A crescentic bar morphology is clearly apparent. A meandering longshore current is seen but it is also seen that the rip-current circulation is very prominent and is able of reversing the longshore current at some locations. For this amplitude of the bathymetric pattern the maximum intensity of the current is 0.5 m s^{-1}. The alongshore migration speed of the spatial pattern is 53 m d^{-1}.

4.2.2. Morfo55

The time evolution up to $t = 100$ d of the bathymetry and the mean current has been computed with MORFO55 starting from the initial bathymetry shown in Fig. 5 plus small perturbations, now for oblique wave incidence. Because of wave refraction, the wave angle in deep water, $\theta_\infty = 10°$, is reduced to $\theta_{x=250} = 6.5°$ at the offshore boundary of the domain. Fig. 13 shows the evolution of the bed level at $x = 50$, $y = 1000$ m. The behaviour is now very different from that displayed in Fig. 8 since now the bed level rises and drops alternatively with an oscillation which increases in amplitude. This reflects the fact that the spatial pattern migrates alongshore while it grows. The final amplitude of the oscillations is about 0.4 m. Their period grows from an initial value of $T = 5$ d up to a final value of $T = 10$ d. Comparing the amplitude of two consecutive maxima at the initial stage, the e-folding time can be estimated as about 5 d.

The bathymetry after 100 d clearly shows a crescentic bar with an alongshore spacing of $\lambda = 250$ m as it is seen in Figs. 12 and 14. In qualitative agreement (at least) with MORFO60 instability mode and with field observations, the longshore current meanders veering offshore at the rip channels and onshore at the shoals. The maximum current intensity is about 0.42 m s^{-1}. The rip-current circulation is quite strong (or the longshore current is rather weak) so that at some points it reverses the direction of the longshore current inducing some vortices. However, the stronger current intensity is not found in the offshore flow but in the onshore flow.

The alongshore migration celerity of the pattern is readily computed as the wavelength divided by the period, being $c \simeq 33$ m d^{-1} at the initial stage and decreasing later on to $c \simeq 21$ m d^{-1}. Thus the initial celerity is comparable to the prediction of the linear stability model although somewhat smaller. This decrease in celerity as the amplitude of the bars becomes larger is quite common (see, e.g., Garnier et al. (2006)).

4.2.3. LEGI model

Again, the final bathymetry is not a crescentic bar for the LEGI model. As it can be seen in Fig. 15, the bar-trough system has been largely smoothed out and the cross-shore profile has become almost terraced. Some alongshore irregularities are present but much less pronounced than in case of normal wave incidence. The circulation is rather irregular with a maximum flow intensity of 0.4 m s^{-1}.

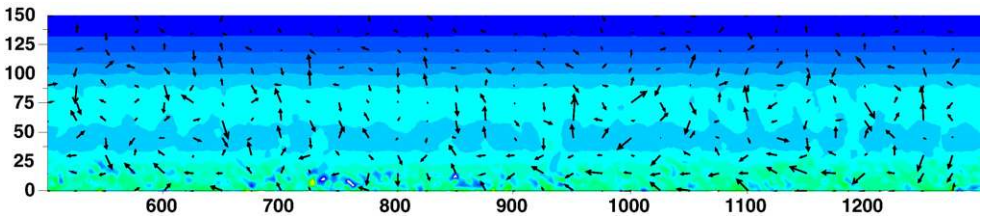

Fig. 15. Bathymetry and circulation after 100 d of morphological evolution computed with the LEGI model for oblique wave incidence. Maximum current intensity: 0.4 m s^{-1}.

4.2.4. LFW-2d

The LWF-2d model has been run over the final bathymetry obtained with MORFO55 now for oblique wave incidence. Fig. 12 shows that the longshore current is very much localized and very strong close to the shoreline its maximum intensity being 1.06 m s^{-1}. The current on the bar is weaker and consistently with MORFO55 it meanders, onshore over the shoals, offshore at the channels. The slight dominance of the onshore directed current over the offshore directed one that was already found with MORFO55 is here enhanced.

5. Discussion

Discussion and conclusions are organized as follows. First a comparison of the models within HUMOR through the test case was presented in the present paper. A survey and overview of morphodynamic models to be applied to surf zone rhythmic topography dynamics from a wider perspective is then presented. Conclusions on our present understanding of the occurrence and dynamics of rhythmic morphologies are given and finally some recommendations.

5.1. Comparison of HUMOR models

Even if MORFO55 is nonlinear and MORFO60 is linear, their results are relatively similar (apart from the fact that the crescentic shape amplitude is undetermined in MORFO60). For normal wave incidence, both predict the formation of a crescentic bar with a very similar spacing (200 and 211 m, respectively). The e-folding time is estimated as 2 d for MORFO55 which is still in the order of the prediction of MORFO60, i.e., 1 d. The rip-current circulation is qualitatively similar and even the maximum current intensities are similar (0.32 m s^{-1} and 0.44 m s^{-1}, respectively). In case of oblique wave incidence the crescentic shape is predicted by both models with a very similar e-folding time: 4 d for MORFO60 and about 5 d for MORFO55. However, a larger difference arises in the spacing which is now 411 m for MORFO60 and 250 m for MORFO55. The prediction of MORFO60 for the alongshore migration celerity of the pattern is 53 m d^{-1} and tends therefore to overestimate the celerity predicted by the nonlinear model at the initial stage, 33 m d^{-1}. As expected, this overestimation is even larger if one compares with MORFO55 prediction for the final stage, 21 m d^{-1}. Interestingly, it seems that the migration celerity is a decreasing function of the amplitude, the linear prediction really holding only for $A \rightarrow 0$. The maximum current intensities are similar, 0.5 m s^{-1} for MORFO60 and 0.42 m s^{-1} for MORFO55. So, our final conclusion here is that since both models are based on the same equations both give relatively similar results no matter they are linear or nonlinear. This holds for the main qualitative features and for the order of magnitude of the spacing, current intensity, characteristic growth time and migration celerity. By assuming that MORFO55 gives the right results and giving to MORFO60 morphological pattern the amplitude predicted by MORFO55, the corresponding error bars in MORFO60 are within 65%.

MORFO55 and LFW-2d coincide on the main qualitative features of the mean hydrodynamics: rip-current circulation in case of normal wave incidence and meandering longshore current in case of oblique wave incidence. Interestingly, the slight reversal of the longshore current at some locations because of the rip-current circulation is predicted by both models even if it is very weak. However, LFW-2d predicts a secondary counter-rotating cell near the coastline which does not occur with MORFO55. Furthermore, that model predicts very strong currents close to the shoreline. Thus, the flow intensities over the bar are similar with both models but the flow velocities near the coastline may reach a factor 2 larger than over the bar for LFW-2d in both cases. This is why maximum flow velocities with LFW-2d are about a factor 2 larger than with MORFO55. This is very likely due to the moving shoreline which does not impose any non-slip condition at the onshore boundary. However, the effect seems to be unrealistically exaggerated as observed currents are not so strong near the shoreline. This is probably due to the crude parameterization of bed shear stress with a constant friction factor, c_d, instead of a coefficient increasing for decreasing water depth. So the model has potential for better describing the hydrodynamics at the shoreline but it turns out that an accurate modelling of bed friction becomes important. Also, comparison with other model runs not shown here suggest that refining the computational mesh may be necessary to obtain good results very close to the shoreline.

Intriguingly, under the same wave conditions and with the same mean hydrodynamic equations, MORFO55/MORFO60 and LEGI model predictions are strikingly different. In case of shore-normal wave incidence, those models predict that the straight bar becomes crescentic with a wavelength of about 200 m and that a rip-current circulation develops. In contrast, in the LEGI model the barred beach tends to become terraced with alongshore irregularities. Some of them resemble shore-normal channels and there is the suggestion of a rough rhythmicity at the scale of some tens of m but there is neither crescentic shape nor clear periodicity. The flow is very irregular and large circulation cells like for MORFO55 do not develop. The reason for this discrepancy should be seek in the different formulation for sediment transport. For example, it has been found that the use of the Bailard (Bailard, 1981) sediment transport formulation in MORFO55 may occasionally suppress the formation of rhythmic bars but this needs a further investigation which was beyond the scope of the HUMOR project. In the case of oblique incidence, the situation is similar, MORFO55 predicting the formation of a crescentic bar and a meandering current while LEGI model does not. In this case the barred beach tends again to become terraced and the alongshore irregularity is less than for normal wave incidence.

5.2. Overview of the models

The HUMOR project has contributed to gaining insight into morphodynamic self-organization processes in the surf zone and, in particular, to understanding the formation and dynamics of rhythmic bars in several ways. First, appropriate models have been developed or extended. Previous modelling efforts of rhythmic bars had used either very idealized models or an

adaptation of commercial models. The former are aimed at capturing the essential physics, but leave many open questions as to the sensitivity to the different factors that are present in nature, or to reliable comparison with observations (see, for instance, Falqués et al., 2000). The latter are more realistic but are, at the same time, rather limited in terms of being able to isolate physical processes. Moreover, it is hard to disentangle physical from numerical effects in models like these, which are in essence a 'black box' (see, for instance, Christensen et al., 1994). The goal of the HUMOR project in this respect has been a step forward in developing models in between. These new models are very flexible in that the user can choose many intermediate options between a highly idealized formulation and a very complex one, which includes all the most relevant processes for the modelling effort. There is still a long way to go in this direction but the present state-of-the-art within the HUMOR project includes: 2DH models where some simplified version of undertow is included; random waves that shoal, refract, diffract, and interact with the currents and break; a number of different descriptions of sediment transport; and a moving shoreline. Another interesting aspect has been the combining and coupling of commercial models with modules constructed *ad hoc*, which are specifically designed to study surf zone bar dynamics (e.g., LEGI model).

Future modelling efforts should address the following issues. Models aimed at describing alongshore rhythmicity are in general unable to predict the equilibrium beach profile or the formation and dynamics of shore-parallel bars. There is clearly a need for improving and including wave-driven cross-shore sediment transport in those models. A first attempt within the project to include undertow and wave asymmetry in the sediment transport has succeeded in modelling the formation of a shore-parallel bar along with the alongshore rhythmicity (Camenen and Larroude, 2003; Fachin and Sancho, 2004b). Recent work by Dronen and Deigaard (in press) also looks at this issue to which further attention must be paid in the future.

Even though the models described in the present paper deal with random waves in height, waves are assumed to be monochromatic and unidirectional. In this respect, the work by Reniers et al. (2004) is pioneering in considering spreading both in frequency and direction for an embayed beach. Also the possibility of nonlinear wave interactions and infragravity wave dynamics is an issue that surf zone models should incorporate, not only for an embayed beach, but also for open coast and oblique wave incidence.

Surf zone transverse/oblique bars are commonly attached to the shoreline at mega-cusps and bar dynamics often linked to shoreline dynamics. However, phase-averaged models coupling shoaling and surf zone morphodynamics and morphological evolution right through to the moving shoreline still need to be developed. The present work on LFW-2d is a significant step along the way. This is non-trivial, but the recent work on characterizing an appropriate shoreline boundary condition for phase-averaged models by Brocchini and Bellotti (2002), Bellotti et al. (2003) and Bellotti and Brocchini (submitted for publication) will aid these developments. Another step forward is the very recent work linked to HUMOR (Stoker and Dodd, 2005) that has succeeded in modelling beach cusp formation using a wave-resolving, 2DH nonlinear (NLSWE) hydrodynamical model coupled with the sediment continuity equation, and incorporating a moving shoreline. The shock-capturing approach taken is highly robust, and rarely results in crashes.

The present research has focused on the use of wave-averaged models. They seem to give reasonable predictions but are missing potentially important phenomena, one of such being an intra-wave description of suspended sediment transport. Over the last few years, several advances have been made using Boussinesq-type models for describing surf zone dynamics. A review of such advances is given in Kirby (2003). Examples of such applications for simulating longshore currents, shear waves and rip-currents are given by Chen et al. (2003) and Chen et al. (1999). A recent morphodynamic application of a wave-resolving model is presented in Dodd et al., submitted for publication. These models can, in principle, be linked with detailed sediment transport formulations, including both bed load and suspended load, and solve simultaneously the bed-updating equation. They do not solve however for the instantaneous vertical velocities, which are fundamental to describe sediment suspension. Also, a detailed boundary layer description could be necessary as such models do not include it. Using such a phase-resolving hydrodynamical description, albeit depth-averaged, is however enormously time-consuming, and so only worth-while pursuing at present when swash zone motions are essential to modelling beach change. Finally, a complete description of the time-varying 3D phenomena is also envisaged, although the relatively large time and space scales at which these morphological bed features form turn this approach impractical.

5.3. Rhythmic bars

As was already known before the HUMOR project, a shore-parallel bar may develop rip channels and become crescentic just by self-organization of the coupling between flow and morphology. This is due to alongshore bed undulations over the bar producing more (less) breaking over the shoals (channels), and this creates a circulation cell with onshore flow over the shoals and offshore flow at the channels. This current carries sediment with it, but the sediment flux has gradients depending on the stirring factor α in the sediment flux, Eq. 11, and on the flow intensity. Because the wave amplitude decreases shoreward over the bar due to wave breaking, α decreases too. This means that the onshore current will bring over the shoals more sediment than that taken out. Similarly, the offshore current will bring less sediment from the channels than that taken out. Thus, there will be deposition at the shoals and erosion at the channels, i.e., there is a positive feedback between the bed undulations and the circulation and associated sediment transport. Actually, since there are gradients in flow intensity due to depth variations, the relevant quantity is not α itself but α/D, the so-called potential stirring (see, e.g., Coco et al., 2002; Garnier et al., 2006).

It is now becoming more and more apparent that crescentic bar formation is a very robust feature in the sense that it is

relatively independent of the various descriptions of waves and sediment transport. In addition to the results presented here (apart from LEGI model outputs) and the HUMOR research of Calvete et al. (2005) this is also supported by Deigaard et al. (1999); Damgaard et al. (2002); Reniers et al. (2004); Klein et al. (2005); Klein (2006); van Leeuwen et al. (2006); Dronen and Deigaard (in press). According to the systematic parameter study of Calvete et al. (2005), the alongshore spacing between crescents increases with distance from bar to shore, with wave height (although it saturates for large waves) and with wave incidence angle. The characteristic formation time increases with wave incidence angle and decreases with increasing wave height (also with saturation for large waves). Interestingly, the suggestion that the exact normal wave incidence could be a singular limit has been now discarded, as a very regular and smooth behaviour is found when increasing the angle from 0 up to 30°. Shoreward of the main circulation cell associated with the rip-currents (offshore directed at the channels and onshore directed on the horns or shoals) a counter-rotating secondary cell very often appears next to the shoreline. This double cell circulation had been observed in wave-basin experiments and in direct hydrodynamic numerical simulations, but never before modelled in the context of crescentic bar formation.

Little attention has so far been paid to the fundamental question of why bars are not always crescentic. Just some clues have been given based on the downslope gravity-driven sediment transport (Caballeria et al., 2002) or a too long growth time in comparison with wave conditions variability in response to, e.g., the mean cross-shore profile and/or wave obliquity (Calvete et al., 2005). Also, the cross-shore profile in potential stirring associated to the different underlying mean bathymetry, sediment characteristics and wave conditions may be very important in that respect. Anyway, this is certainly an important aspect for future research.

The contributions within HUMOR have provided more evidence that shore-transverse and oblique sand bars may emerge too from the self-organized coupling between flow and morphology, even when a more realistic modelling framework is adopted. Nevertheless, the large diversity of the results depending on wave description and, especially, sediment transport formulation suggests that the formation of such bars is a very complex process, which depends critically on many factors (Ribas et al., 2003; Klein, 2006; van Leeuwen et al., 2006). Additionally, comparisons between linear stability and initial development in nonlinear models give qualitative agreement but also some quantitative differences hardly explainable by the minor differences in model equations (comparisons MORFO60, MORFO55 and M-SHORECIRC, not shown here). Notwithstanding all these difficulties, the gradients in potential stirring, α/D, provide a quite general tool to predict and understand transverse/oblique bar formation (Garnier et al., 2006). Oblique down-current oriented bar formation is associated with an offshore directed gradient in potential stirring in the inner surf zone and an onshore deflection of the longshore current over the bars. This can be understood by arguments that are similar to those stated for crescentic bars. Likewise, oblique up-current oriented bar formation is associated with an onshore directed gradient in potential stirring and an offshore deflection of the current over the bars. Transverse bars seem to occur for normal wave incidence when there is an offshore directed gradient in potential stirring. When the sediment transport driven by waves and currents is not in the direction of the current, so α is an anisotropic tensor, the behaviour may be much more complex (Ribas et al., 2005).

In spite of such complications, nonlinear models developed within HUMOR have been successful in some cases in describing the growth of oblique/transverse bars up to finite amplitude. In some cases, saturation of the growth is obtained and the final amplitude (not necessarily constant but pulsating) can be predicted (Garnier et al., 2006). Typical nonlinear phenomena as the final asymmetric shape and splitting or merging of bars is likewise reproduced. Lastly, though not the focus of this contribution, HUMOR has also led to the first process-based (nonlinear) modelling of beach cusp evolution (Stoker and Dodd, 2005), previously only described by a cellular automata model (Coco et al., 2000).

5.4. Recommendations

Recommendations arising from the HUMOR project for future field experiments are necessarily tentative, not least because this project has been concerned with modelling and the understanding of the physics gained thereby. Nevertheless, model developments within HUMOR indicate very clearly that there is a crucial need for field measurements of sediment transport. Most of the sediment transport formulations used within the present models have actually not been calibrated under the environments of interest. For instance, an important issue for morphodynamic models seems to be that the sediment flux (driven by waves and current) may be in a direction which is different from the direction of the mean current. Also, the contribution of the bed slope to the total transport is another important aspect since this is likely one of the factors suppressing alongshore rhythmicity for high energy conditions (Caballeria et al., 2002). A better knowledge of the wave stirring function derived from field measurements is strongly desirable, and, in particular, its gradient and extrema. Previous comprehensive field campaigns, such as those at Duck, are likely already to have collected some measurements that contain relevant information. However, disentangling sediment transport (bed- and suspended load) due to waves and currents, as well as due to two or three dimensional effects, is likely to be very difficult. Further experiments, with perhaps extensive measurements in regions of the cross-shore profile where the stirring function gradient is likely to be high, may be useful.

Detailed experiments should also aim at assessing more accurately the bed shear stresses and the turbulent mixing in the surf and swash zones, both on planar and barred beaches, as these are important terms in the hydrodynamical governing equations and their present formulation is no more than a simple approximation.

On a larger scale ARGUS imaging has proven invaluable in observing complex beach patterns and evolution. The main missing ingredient is three dimensionality. One of the next tasks

for remote sensing will be to obtain synoptic images of actual bathymetry, in much the same way that ARGUS now allows us a two dimensional picture of dissipation and therefore shoals. LIDAR goes some way to achieving this already, but breaking (turbidity) and biological factors and sediments within the water column act to obscure the picture. Land-based methods will also provide more comprehensive (and cheaper) data-sets. Perhaps, in the short term, even more important is the nearshore circulation. In situ measurements, however intensive, can never give the same intuitive understanding of circulation that remote sensing can, were an appropriate technique to be developed. It must be emphasized, however, that these are long term goals and very substantial developments.

Physical modelling could also help addressing some open questions. Presently available state-of-the-art 3-dimensional experimental facilities, capable of generating both waves and currents, have dimensions typically of the order of 30 to 50 m. This means that we could expect to be able to simulate prototype lengths if the order of 1000 m, for model-to-prototype scales around 1:30. This does not seem to pose a problem, but difficulties may arise regarding appropriate scaling laws for the sediments, simulating large time scales in order to have natural bed features, and dealing with appropriate boundary conditions within the basins for both currents and sediments.

Acknowledgments

This publication is part of the HUMOR project, funded by the European Commission under Contract No. EVK3-2000-22014-HUMOR. R. Garnier thanks the Catalan Government for his IQUC grant. F. Ribas developed the work presented here partly during her one-year research position at IMAU, Utrecht University. Funding of the work by F. Ribas and D. Calvete from the Spanish Government through the 'Juan de la Cierva' and 'Ramon y Cajal' programs, respectively, is gratefully acknowledged. L.C. MacHardy and N. Dodd also gratefully acknowledge the support of HR Wallingford Ltd. and The University of Nottingham.

References

Ashton, A., Murray, A.B., Arnault, O., 2001. Formation of coastline features by large-scale instabilities induced by high-angle waves. Nature 414, 296–300.

Bailard, J.A., 1981. An energetics total load sediment transport model for a plane sloping beach. J. Geophys. Res. 86 (C11), 10938–10954.

Battjes, J.A., 1975. Modeling of turbulence in the surfzone. Proc. Symp. Model. Techn. A.S.C.E., San Francisco, U.S.A., pp. 1050–1061.

Bellotti, G., Archetti, R., Brocchini, M., 2003. Experimental validation of characterization of mean swash zone boundary conditions. J. Geophys. Res. 108 (C8), C3250. doi:10.1029/2002JC001510.

Bellotti, G., Brocchini, M., submitted for publication. Swash zone boundary conditions for long wave models. Coastal Eng. Submitted, special issue on DELOS.

Bijker, E.W., 1968. Littoral drift as function of waves and current. Coastal Eng. 1968. Am. Soc. of Civ. Eng., pp. 415–435.

Blondeaux, P., 2001. Mechanics of coastal forms. Annu. Rev. Fluid Mech. 33, 339–370.

Brocchini, M., Bellotti, G., 2002. Integral flow properties of the swash zone and averaging. Part 2. The shoreline boundary conditions for wave-averaged models. J. Fluid Mech. 458, 269–281.

Caballeria, M., Coco, G., Falqués, A., Huntley, D.A., 2002. Self-organization mechanisms for the formation of nearshore crescentic and transverse sand bars. J. Fluid Mech. 465, 379–410.

Calvete, D., Dodd, N., Falqués, A., 2002. Morphological development of nearshore bed-forms. In: Smith, J.M. (Ed.), Coastal Eng. 2002, vol. 3. World Scientific, Singapore, pp. 3321–3332.

Calvete, D., Dodd, N., Falqués, A., van Leeuwen, S.M., 2005. Morphological development of rip channel systems: normal and near normal wave incidence. J. Geophys. Res. 110 (C10006). doi:10.1029/2004JC002803.

Camenen, B., Larroude, P., 2003. Un modéle morphologique côtier pour la création de barres rythmiques. Revue Française de génie civil 7/9, 1099–1116.

Carter, R.W.G., 1988. Coastal Environments. Academic Press.

Castelle, B., 2004. Modélisation de l'hydrodynamique sédimentaire au-dessus des barres sableuses soumises á l'action de la houle: application á la côte aquitaine. Ph.D. thesis, Université Bordeaux I, France.

Chen, Q., Dalrymple, R.A., Kirby, J.T., Kennedy, A.B., Haller, M.C., 1999. Boussinesq modelling of a rip current system. J. Geophys. Res. 104, 20617–20637.

Chen, Q., Kirby, J.T., Dalrymple, R.A., Shi, F., Thornton, E.B., 2003. Boussinesq modeling of longshore currents. J. Geophys. Res. 108 (C11). doi:10.1029/2002JC001308.

Christensen, E., Deigaard, R., Fredsoe, J., 1994. Sea bed stability on a long straight coast. In: Edge, B.L. (Ed.), Coastal Eng. 1994, vol. 4. Am. Soc. of Civ. Eng., New York, U.S.A., pp. 1865–1879.

Church, J.C., Thornton, E.B., 1993. Effects of breaking wave induced turbulence within a longshore current model. Coast. Eng. 20, 1–28.

Coco, G., Caballeria, M., Falqués, A., Huntley, D.H., 2002. Crescentic bars and nearshore self-organization processes. In: Smith, J.M. (Ed.), Coastal Engineering 2002, vol. 3. World Scientific, Singapore, pp. 3765–3777.

Coco, G., Huntley, D.A., O, Hare, T.J., 2000. Investigation of a self-organization model for beach cusp formation and development. J. Geophys. Res. 105 (C9), 21991–22002.

Damgaard, J., Dodd, N., Hall, L., Chesher, T., 2002. Morphodynamic modelling of rip channel growth. Coast. Eng. 45, 199–221.

Deigaard, R., Drønen, N., Fredsoe, J., Jensen, J.H., Jørgesen, M.P., 1999. A morphological stability analysis for a long straight barred coast. Coastal Eng. 36 (3), 171–195.

Dodd, N., Blondeaux, P., Calvete, D., de Swart, H.E., Falqués, A., Hulscher, S.J.M.H., Różyński, G., Vittori, G., 2003. The use of stability methods in understanding the morphodynamical behavior of coastal systems. J. Coast. Res. 19 (4), 849–865.

Dodd, N., Stoker, A.M., Garnier, R., Vittori, R., De Los Santos, F., Brocchini, M., Soldini, L., Losada, M.A. 2008. Use of numerical models to study land-based sedimentation and subsequent nearshore morphological evolution. Coastal Eng. 55, 608–618.

Dronen, N., Deigaard, R., in press. Quasi-three-dimensional modelling of the morphology of longshore bars. Coast. Engineering 54.

Evans, O.F., 1938. The classification and origin of beach cusps. J. Geol. 46, 615–627.

Evans, O.F., 1939. Mass transportation of sediments on subaqueous terraces. J. Geol. 47, 325–334.

Fachin, S., Sancho, F., 2004a. M-shorecirc: a new morphodynamical model. Presented at International Coastal Symposium— ICS 2004. To appear in J. Coastal Res., Special Issue 39.

Fachin, S., Sancho, F., 2004b. Morphodynamic instabilities in the surf zone. In: Smith, J.M. (Ed.), Coastal Engineering 2004, Proceedings of the 29th Intl. Conference. ASCE, Lisbon, pp. 2875–2887.

Falqués, A., 1989. Formacion de topografía rítmica en el Delta del Ebro. Rev. Geofis. 45 (2), 143–156.

Falqués, A., Coco, G., Huntley, D.A., 2000. A mechanism for the generation of wave-driven rhythmic patterns in the surf zone. J. Geophys. Res. 105 (C10), 24071–24088.

Falqués, A., Montoto, A., Iranzo, V., 1996. Bed-flow instability of the long-shore current. Cont. Shelf Res. 16 (15), 1927–1964.

Garnier, R., Calvete, D., Falqués, A., Caballeria, M., 2006. Generation and nonlinear evolution of shore-oblique/transverse sand bars. J. Fluid Mech. 567, 327–360.

Guilcher, A., Godard, A., Visseaux, E., 1952. Les cretes et sillons obliques de l'estran des Landes de Gascogne. Comite d'Oceanogr. et d'Etudes des Cotes Bull. 4 (4), 151–157.

Hamm, L., Capobianco, M., Dette, H.H., Lechuga, A., Spanhoff, R., Stive, M.J.F., 2002. A summary of European experience with shore nourishment. Coast. Eng. 47, 237–264.

Hino, M., 1974. Theory on formation of rip-current and cuspidal coast. Coastal Eng. 1974. Am. Soc. of Civ. Eng., New York, U.S.A., pp. 901–919.

Holman, R.A., Bowen, A.J., 1982. Bars, bumps, and holes: models for the generation of complex beach topography. J. Geophys. Res. 87 (C1), 457–468.

Homma, M., Sonu, C., 1962. Rhythmic pattern of longshore bars related to sediment characteristics. Coastal Eng. 1962. Am. Soc. of Civ. Eng., pp. 248–278.

Hubbard, M.E., Garcia-Navarro, P., 2000. Flux difference splitting and the balancing of source terms and flux gradients. J. Comput. Phys. 165 (1), 89–125.

Hunter, R.E., Clifton, H.E., Phillips, R.L., 1979. Depositional processes, sedimentary structures, and predicted vertical sequences in barred nearshore systems, Southern Oregon coast. J. Sediment. Petrol. 49 (3), 711–726.

Kirby, J.T., 2003. Boussinesq models and applications to nearshore wave propagation, surf zone processes and wave-induced currents. In: Lakhan, C. (Ed.), Advances in Coastal Modeling. Elsevier Science B.V., pp. 1–41.

Kirby, J.T., Dalrymple, R.A., 1994. Combined refraction/diffraction model REF/DIF1, Version 2.5. Res. Report CACR-94-22, Center for Applied Coastal Research. Univ. of Delaware.

Klein, M.D., 2006. Modelling rhythmic morphology in the surf zone. Ph.D. thesis, Tech. Univ. Delft, The Netherlands.

Klein, M.D., Schuttelaars, H.M., Stive, M.J.F., 2005. Influence of sediment transport formulation on the linear stability of planar and barred coasts. In: Smith, J.M. (Ed.), Coastal Eng. 2004, vol. 3. World Scientific, pp. 2716–2728.

Komar, P.D., 1998. Beach Processes and Sedimentation, 2nd Edition. Prentice Hall.

Konicki, K.M., Holman, R.A., 2000. The statistics and kinematics of transverse bars on an open coast. Mar. Geol. 169, 69–101.

Lafon, V., Dupuis, H., Howa, H., Froidefond, J.M., 2002. Determining ridge and runnel longshore migration rate using spot imagery. Oceanol. Acta 25, 149–158.

Larroudé, P., Camenen, B., 2004. 2DH and multi1DH morphological model for medium term evolution of large scale features and nourishment in the nearshore region: application to TrucVert and Corniche beach (France) and la Barrosa beach (Spain). 29th International Conference on Coastal Engineering. ASCE, Lisbon.

Lee, C., Park, W.S., Cho, Y., Suh, K.D., 1998. Hyperbolic mild-slope equations extended to account for rapidly varying topography. Coast. Eng. 34, 243–257.

Lippmann, T.C., Holman, R.A., 1990. The spatial and temporal variability of sand bar morphology. J. Geophys. Res. 95 (C7), 11575–11590.

LNHE-Chatou, 2002a. Sisyphe— modelisation system of telemac, version 5.2-user-validation manual. Tech. rep., Edf-Gdf.

LNHE-Chatou, 2002b. Telemac2d— modelisation system of telemac, version 5.2-user-validation manual. Tech. rep., Edf-Gdf.

Niederoda, A.W., Tanner, W.F., 1970. Preliminary study on transverse bars. Mar. Geol. 9, 41–62.

Pedreros, R., Howa, H.L., Michel, D., 1996. Application of grain size trend analysis for the determination of sediment transport pathways in intertidal areas. Mar. Geol. 135, 35–49.

Putrevu, U., Svendsen, I.A., 1999. Three-dimensional dispersion of momentum in wave-induced nearshore currents. Eur. J. Mech. B, Fluids 83–101.

Reniers, A.J.H.M., Roelvink, J.A., Thornton, E.B., 2004. Morphodynamic modeling of an embayed beach under wave group forcing. J. Geophys. Res. 109 (C01030). doi:10.1029/2002JC001586.

Ribas, F., Falqués, A., Montoto, A., 2003. Nearshore oblique sand bars. J. Geophys. Res. 108 (C4), 3119. doi:10.1029/2001JC000985.

Ribas, F., Kroon, A., submitted for publication. Characteristics and dynamics of transverse finger bars. J. Geophys. Res. Submitted.

Ribas, F., Vis-Star, N., Swart, H., Falqués, A., 2005. Generation of nearshore oblique sand bars: sensitivity to sand transport formulation. In: Smith, J.M. (Ed.), Coastal Eng. 2004, vol. 3. World Scientific, pp. 2888–2900.

Ruessink, B.G., van Enckevort, I.M.J., Kingston, K.S., Davidson, M.A., 2000. Analysis of observed two- and three-dimensional nearshore bar behaviour. Mar. Geol. 169, 161–183.

Sancho, F.E.P., 1998. Unsteady nearshore currents on longshore varying topographies. Ph.D. thesis, University of Delaware, Dept. of Civil Engineering.

Short, A.D., 1999. Handbook of Beach and Shoreface Morphodynamics. Wiley, Chichester.

Sonu, C.J., 1972. Field observation of nearshore circulation and meandering currents. J. Geophys. Res. 77 (18), 3232–3247.

Sonu, C.J., 1973. Three-dimensional beach changes. J. Geology 81, 42–64.

Soulsby, R.L., 1997. Dynamics of Marine Sands. Thomas Telford, London, U.K.

Spanhoff, R., Biegel, E.J., Burger, M., Dunsbergen, D.W., 2003. Shoreface nourishments in The Netherlands. Coastal Sediments 2003. World Scientific, Corpus Christi, Texas, USA.

Stoker, A.M., Dodd, N., 2005. Evolution of beach cusps. Proceedings of Coastal Dynamics 2005. Barcelona, p. To appear.

Svendsen, I., 1984. Mass flux and undertow in the surf zone. Coast. Eng. 8, 347–365.

Svendsen, I.A., Haas, K., Zhao, Q., 2001. Quasi-3d nearshore circulation model shorecirc. Version 1.3.6. Res. report, Center for Applied Coastal Research. Univ. of Delaware.

Toro, E.F., 1997. Riemann solvers and numerical methods for fluid dynamics. Springer, Berlin.

Van Dongeren, A.R., Sancho, F.E.P., Svendsen, I.A., Putrevu, U., 1994. Shorecirc: a quasi-3d nearshore model. 24th Int. Conf. Coastal Engng., vol. 3. ASCE, Kobe, pp. 2741–2754.

van Enckevort, I.M.J., 2001. Daily to yearly nearshore bar behaviour. Ph.D. thesis, Netherlands Geographical Studies, University of Utrecht, Utrecht, The Netherlands.

van Enckevort, I.M.J., Ruessink, B.G., Coco, G., Suzuki, K., Turner, I.L., Plant, N.G., Holman, R.A., 2004. Observations of nearshore crescentic sandbars. J. Geophys. Res. 109 (C06028). doi:10.1029/2003JC002214.

van Leeuwen, S.M., Dodd, N., Calvete, D., Falqués, A., 2006. Physics of nearshore bed pattern formation under regular or random waves. J. Geophys. Res. 111 (F01023). doi:10.1029/2005JF000360.

Wright, L.D., Short, A.D., 1984. Morphodynamic variability of surf zones and beaches: a synthesis. Mar. Geol. 56, 93–118.

Yu, J., Slinn, D.N., 2003. Effects of wave–current interaction on rip currents. J. Geophys. Res. 108 (C3), 3088. doi:10.1029/2001JC001105.